Journal of Catalysis 278 (2011) 123–132

Contents lists available at ScienceDirect

Journal of Catalysis

journal homepage: www.elsevier.com/locate/jcat

Structural effects of Na promotion for high water gas shift activity on Pt–Na/TiO_2

Xinli Zhu, Min Shen, Lance L. Lobban, Richard G. Mallinson *

Center for Biomass Refining, School of Chemical, Biological, and Materials Engineering, The University of Oklahoma, Norman, OK 73019, USA

ARTICLE INFO

Article history:
Received 17 September 2010
Revised 24 November 2010
Accepted 30 November 2010
Available online 11 January 2011

Keywords:
Water gas shift
Pt–Na/TiO_2
Platinum
Titania
Sodium
Hydrogen
Strong metal–promoter interaction

ABSTRACT

Sodium (1–10 wt.%)-promoted 1 wt.% Pt/TiO_2 catalysts were prepared by a co-impregnation method and tested for the water gas shift (WGS) reaction under differential reaction conditions. Significantly higher intrinsic activity is achieved with 2–4 wt.% Na addition, when 2–4 layers of NaO_x are deposited on the support and the Pt particles are partially covered by NaO_x, with moderate surface basicity and exposed Pt surface areas. In addition to the physical coverage, XPS data suggest that interactions between Pt and NaO_x may occur by Pt electron donation to O in NaO_x through Pt–O–Na. The strong metal–promoter interactions provide highly active sites for the WGS reaction at the periphery of the Pt–NaO_x interface and also inhibit Pt particles from sintering. Optimal 4 wt.% Na (Na/Pt = 34) improves the intrinsic reaction rate and turnover frequency of Pt/TiO_2 at 300 °C by 8 and 11 times, respectively, and appears to be significantly higher than reported in the literature.

The catalysts were characterized by X-ray diffraction, N_2 adsorption, CO chemisorption, transmission electron microscopy, H_2 temperature-programmed reduction, CO_2 temperature-programmed desorption, and X-ray photoelectron spectroscopy.

1. Introduction

The demand for hydrogen production for relatively small-scale applications appears to be of increasing importance for future energy systems, such as for hydrogen proton exchange membrane fuel cells for power generation and hydrogen production processes for small and distributed bio-fuel refinery plants. The water gas shift (WGS) reaction is one of the key components of hydrogen production systems that convert CO and H_2O from reforming and other conversion streams (biomass, gasification, etc.) to CO_2 and additional H_2:

$$CO + H_2O \leftrightarrow CO_2 + H_2, \quad \Delta H = -41.2\ \text{kJ/mol}.$$

The slightly exothermic property of this reaction makes CO conversion strongly limited by thermodynamics at high temperatures and by kinetics at low temperatures. To overcome these limitations, two-stage WGS reactors are operated industrially with a low space velocity of 3000 h^{-1} for low temperature shift (due to the low thermal stability of Cu-based catalysts) [1]. This configuration is difficult to apply on a small scale because of the large reactor volume as well as the pyrophoric property of the usual Cu-based catalysts. Alternatively, a single-stage WGS reactor operated at medium temperatures of 250–300 °C with CO conversion approaching equilibrium could be an alternative approach for improved processes. Active and stable catalysts capable of frequent startup–shutdown are desirable to achieve high space velocity operations of 40,000 h^{-1} (consequently, smaller reactor volume) [1]. Noble metal (Pt and Au) catalysts supported on reducible oxides (ceria and titania) have received extensive attention recently [1–3].

Numerous studies have shown Pt/CeO_2 and Pt/TiO_2 to be the most active Pt-based catalysts for the WGS reaction [4–9]. Addition of promoters (such as Re [9–13], Mg [14], V [15], Ce [16–18], Mo [19]) and incorporation of ZrO_2 into CeO_2 [9,20] improve the activity, but usually by less than a factor of 3. Table 1 lists recent literature that reports reaction rate and/or turnover frequency (TOF) of promoted Pt/TiO_2 and Pt/CeO_2 for the WGS reaction.

Alkali metals are widely used as promoters of catalysts for many reactions, including WGS catalysts [2]. For example, Campbell and coworkers demonstrated that introduction of Cs to Cu(1 1 0) enhanced the WGS rate by a factor of 5 due to the enhancement of H_2O activation over Cs [21]. An alkali-promoted noble metal catalyst was reported by Sato and White [22]. Addition of 4 wt.% NaOH coatings to 3%Pt/TiO_2 enhanced the photocatalytic WGS reaction rate by a factor of 2.5. The maximum H_2 production rate was obtained with a 7 wt.% NaOH coating, but with some contributions from photolysis of H_2O. Pigos et al. [23,24] reported that alkali doping significantly improves the WGS activity of Pt/ZrO_2 (3–4%Pt/3%Na/2%V/ZrO_2 and 2%Pt/2.5%Na/ZrO_2 or equimolar for other alkalis) because alkaline species facilitate the C–H bond cleavage of formate, which is believed to be the rate determining step for the overall reaction. Evin et al. [25,26] reported similar improvement in WGS activity for a Pt/CeO_2 catalyst via alkali doping as a result of enhancement of C–H cleavage of formate. The authors also observed that there was an optimum alkali loading (2%Pt/0.5%Na/CeO_2 or equimolar for other alkalis) to maximize

* Corresponding author. Fax: +1 405 325 5813.
E-mail address: mallinson@ou.edu (R.G. Mallinson).

0021-9517/$ - see front matter © 2010 Elsevier Inc. All rights reserved.
doi:10.1016/j.jcat.2010.11.023

Table 1
Comparison of water gas shift reaction rate and turnover frequency of promoted Pt/TiO_2 and Pt/CeO_2 catalysts reported in the literature.

Catalyst	Compositions (%)	Reaction temperature (°C)	Reaction rate ($\mu mol\ g_{cat}^{-1}\ s^{-1}$)	Turnover frequency (s^{-1})	Reference
Pt/TiO_2	3%CO–7.5%H_2O–89.5%N_2	300	95		9
$Pt–Re/TiO_2$	(2 bar pressure)	300	125		9
Pt/CeO_2	6%CO–60%H_2O–16%H_2–	300	1.89		14,15
$Pt/MgO–CeO_2$	1.6%CO_2–0.4%CH_4–	300	2.80		14
$Pt/6VCeO_2$	16%N_2	300	3.81		15
Pt/TiO_2	6.3%CO–37.5%H_2O–	280	7.18	0.44	17
$Pt/Ce/TiO_2$	6.3CO_2–49.9%H_2	280	19.4	0.65	17
Pt/TiO_2	3%CO–10%H_2O–87%He	250	10.3	0.51	28
$Pt/Na/TiO_2$		250	38.4	1.58	28
Pt/TiO_2	2.83%CO–5.66%H_2O	300	6.98	0.36	13, a
$Pt–Re/TiO_2$	–37.7%H_2–53.8%He	300	10.83	0.35	13
$Pt–4Na/TiO_2$		300	58.6	3.82	a

a: Current work.

the WGS reaction rate. It is not clear how many times the intrinsic reaction rate is improved for the alkali-promoted Pt/ZrO_2 and Pt/CeO_2 catalysts. It is noted that these catalysts were prepared by a sequential impregnation method. Very recently, Panagiotopoulou and Kondarides reported alkali-promoted Pt/TiO_2 catalysts for the WGS reaction, also prepared by a sequential impregnation [27,28]. Their results showed a maximum improvement in turnover frequency of 3 times was achieved for Na-promoted Pt/TiO_2 catalysts with a molar Pt/Na ratio of 1 (0.5%Pt/0.06%Na/TiO_2). They correlated the WGS activity with the H_2 desorption temperature, which is varied by the incorporation of alkalis producing new sites at the metal–support interface (metal–oxygen vacancy–Ti^{3+}).

It is noted that the molar Na/Pt ratio is lower than 10 in those studies [23–28]. There has been no study presented with higher Na/Pt ratios. While those previous studies have used sequential impregnation, it is expected that co-impregnation may have a profound influence on the structures of the support surface, metal surface, metal–support interface, as well as bulk metal particles. In previous work, we have reported that the WGS activity of Pt/TiO_2 was significantly improved by the addition of Na prepared by co-impregnation [29]. 1%Pt–3%Na/TiO_2 was found to be capable of reducing the CO concentration from 30% CO to 0.52% at 300 °C with a space velocity up to 40,000 $cm^3 \cdot g_{cat}^{-1} \cdot h^{-1}$ (dry basis). Furthermore, the catalyst was quite stable at reaction temperatures higher than 250 °C. In the present work, we have measured the intrinsic reaction rate under differential reaction conditions, showing that the improvement in WGS activity for the optimized Na loading is as high as 8 times. Characterizations have been performed to show the structural changes that lead to this significant improvement in WGS activity.

2. Experimental

2.1. Catalyst preparation

The sodium-promoted Pt/TiO_2 catalysts were prepared by co-impregnation of TiO_2 (Degussa P25, BET surface area 49 m^2/g) with aqueous $NaNO_3$ (Aldrich) and $H_2PtCl_6 \cdot 6H_2O$ (Aldrich) overnight [29]. The resulting samples were dried at 110 °C for 12 h followed by calcination in flowing air at 400 °C for 4 h. The Pt loading was fixed at 1 wt.%. The amount of Na loading was varied from 0% to 10 wt.%. These samples are denoted as Pt–*x*Na, where *x* is the weight percentage of Na loading.

2.2. Characterization

The specific surface area was measured by nitrogen adsorption in an ASAP 2000 analyzer (Micromeritics) at −196 °C after outgassing the samples under vacuum at 350 °C for 3 h.

X-ray powder diffraction (XRD) patterns of the catalyst samples were recorded by a Bruker D8 Discover diffractometer, with a Cu Kα radiation source (λ = 1.54056 Å). The crystallite size of TiO_2 was estimated from the full width at half maximum of the diffraction peaks using the Scherrer formula.

Transmission electron microscopy (TEM) and high resolution TEM (HR-TEM) observations were performed on a Philips JEOL 2000-FX system and a JEOL 2010F field emission system, respectively. Both instruments were operated at 200 kV, with magnification varied 400–1200 k times. The fine catalyst powder (which was pre-reduced at 300 °C for 1 h) was dispersed ultrasonically in ethanol. A drop of the suspension was deposited on a carbon-coated copper grid for TEM analysis. The surface-weighted particle size d_s was calculated by the following formula: $d_s = \sum n_i d_i^3 / \sum n_i d_i^2$, where d_i is the particle size of n_i particle. Approximately 200 particles from different TEM photographs of the sample were used to calculate the d_s.

CO chemisorption, H_2 temperature-programmed reduction (H_2-TPR), and CO_2 temperature-programmed desorption (CO_2-TPD) were performed in a temperature-programmed system consisting of a gas delivery system (manifolds and flow meters), oven with temperature controller, micro quartz reactor (1/4 in. o.d.), six-port valve, and thermal conductivity detector (TCD, SRI 310C GC) or Cirrus mass spectrometer (MS, MKS).

CO chemisorption was measured by a dynamic pulse method. The sample (50 mg, 40–60 mesh) was reduced at 300 °C for 1 h in flowing H_2, followed by flushing in He (30 mL/min) for 0.5 h to desorb H_2. Then, the temperature was lowered to room temperature in He flow. Pulses of 5% CO/He (100 μL) was introduced to the catalyst until uptake saturation was obtained. The dispersion of Pt was calculated assuming CO/Pt stoichiometric ratio of 1.

For H_2-TPR, the catalyst sample (20 mg) was subjected to flow of 5% H_2/Ar at room temperature for 3 h to stabilize the TCD signal. After that, the temperature was ramped to 800 °C with a rate of 10 °C/min. The H_2 consumption was monitored by TCD after produced H_2O removal. The H_2 consumption was calibrated by CuO reduction.

For CO_2-TPD, the catalyst sample (100 mg) was reduced at 300 °C for 1 h in flowing H_2, followed by flushing in He for 0.5 h to desorb H_2. The temperature was then lowered to 100 °C in He flow for CO_2 adsorption for 0.5 h. After that, He flowed for 0.5 h to remove weakly adsorbed CO_2. To conduct the TPD, the temperature was increased to 700 °C at a heating rate of 10 °C/min. The evolution of desorbed species was continuously monitored by MS signals at m/z = 2, 18, 28, and 44. The quantification of MS signals was performed using 100 μL pulses of CO and CO_2.

X-ray photoelectron spectroscopy (XPS) measurements were recorded on a Physical Electronics PHI 5800 ESCA system, equipped with an Al Kα X-ray anode operated at 350 W and 15 kV. The base

pressure of the main chamber was kept at about 1.0×10^{-8} Torr. The pass energy was set as 50 eV for all the measurements. The spectra were referenced to Ti $2p_{3/2}$ at a binding energy (BE) of 490.0 eV for TiO_2. The surface composition was estimated from the integrated intensities corrected by atomic sensitive factors.

2.3. Catalytic activity measurements

The catalytic activity was evaluated under differential reaction conditions using a 1/4 in. o.d. quartz reactor at atmospheric pressure. The catalyst sample (40–60 mesh) was reduced at 300 °C in flowing H_2 before shifting to reactant gases at the desired reaction temperature. The dry gas components were 3%CO–57%He–40%H_2. The gas flow rate was varied from 30 to 500 cm^3/min controlled by mass flow controllers; H_2O was fed by a syringe pump and vaporized before entering the reactor. H_2O flow rate was adjusted with gas flow rate to keep H_2O/CO ratio at 2 for all runs (resulting in a wet basis composition of 2.83%CO–5.66%H_2O–37.74%H_2–53.77%He). The catalyst (10–100 mg) was mixed with α-Al_2O_3 (which was verified to be inert under reaction conditions) to get a total weight of 100 mg. These conditions allowed the CO conversion to be kept to less than 10%. The gases (H_2, CO_2, CO, and possibly CH_4) after reaction were analyzed online by a Carle AGC 400 gas chromatograph (with HTS hydrogen analysis system and a TCD) after passing through a cold trap to remove water. No CH_4 was detected in any experiment. No deactivation was observed under current reaction conditions. Results are reported on a dry gas basis. The reaction rate (r) is defined as moles of CO converted per gram of catalyst per second. The turnover frequency (TOF) is defined as moles of CO converted per mole of Pt surface atoms per second. The surface Pt atoms were estimated from the dispersion derived from CO chemisorption.

3. Results and discussion

3.1. Characterizations

3.1.1. Textural structure

Fig. 1 shows the XRD patterns of selected samples. The diffraction peaks at $2\theta = 25.3°$, 37.9°, 48.4°, 53.9°, 55.3°, 62.7°, 69.0°, 70.2° are related to anatase (~80%); while peaks at $2\theta = 27.5°$, 36.0°, 54.2°, 62.3° are assigned to rutile (~20%). The average crystallite sizes of TiO_2 are ~17 nm for anatase and ~23 nm for rutile. The crystallite sizes are not influenced by the loading of Pt or Na. No

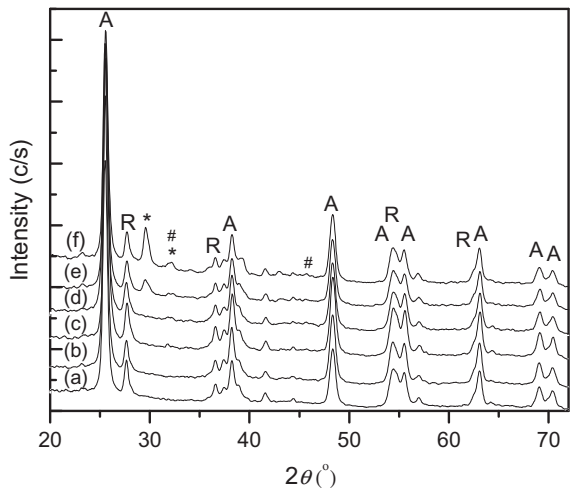

Fig. 1. XRD patterns of (a) TiO_2; (b) Pt–0Na; (c) Pt–1Na; (d) Pt–3Na; (e) Pt–6Na; (f) Pt–10Na. A, Anatase; R, Rutile; ∗, $NaNO_3$, # may be assigned to NaCl, Na_2O, NaO_2.

Pt species (Pt^0, PtO, PtO_2) are observed, indicating that Pt species are highly dispersed on the support. At high Na loadings (Pt–6Na and Pt–10Na), residual un-decomposed $NaNO_3$ (PDF #00-001-0840) diffraction peaks are observed at $2\theta = 29.4°$ and 31.8° (further supported by XPS, see below), implying excess Na loading for these samples. The peak intensity of $NaNO_3$ is much weaker in Pt–Na/TiO_2 samples than in Na/TiO_2 samples (Fig. S1) with the same amount of Na loading, indicating that Pt catalyzed the decomposition of $NaNO_3$ during calcination. The peak intensity for $2\theta = 32°$ is stronger for Pt–Na/TiO_2 samples than for Na/TiO_2 samples (Fig. S1), accompanied by the appearance of a peak at $2\theta = 45°$, implying the formation of small amounts of NaCl (PDF #00-005-0628), Na_2O (PDF #03-065-2978), and NaO_2 (PDF #01-077-0207). These all have major diffraction peaks at $2\theta = 32°$ and 45°.

The BET specific surface areas (S_{BET}) and total pore volumes (V_p) of Pt–Na/TiO_2 catalysts are listed in Table 2. It is seen that both S_{BET} and V_p decrease with increasing Na loading. The influence of Na is small at low loading (1%), but is pronounced at high loading (>6%), as a result of Na species coverage of the TiO_2 support.

3.1.2. Pt dispersion

The Pt dispersion is determined by CO chemisorption, and the results are shown in Table 2. The Pt dispersion for the Pt–0Na sample (38.5%) is higher than all Na-promoted samples. The highest Pt dispersion (~30%) for a Na-promoted sample is obtained for 2–4 wt.% Na loading. Na loading lower or higher than this range lowers the Pt dispersion, perhaps due to Na species coverage.

TEM observations were carried out to differentiate whether the variation in dispersion is due to Pt particle size or Na species coverage. Representative TEM images of Pt–0Na, Pt–1Na, Pt–3Na, and Pt–10Na are displayed in Fig. 2, and the derived particle size distributions are shown in Fig. 3. Low Na loading (Pt–1Na, 1.6 nm) has little effect on Pt particle size distributions compared to the Pt only sample (Pt–0Na, 1.6 nm). The particle size distribution is broadened with increased Na loading. The average Pt particle size increases to 2.0 and 2.4 nm, with Na loading increasing to 3% and 10%, respectively. These findings are in accordance with literature showing that slight Pt [30] and Pd [31] particle size growth with high amount of alkali loadings. The sharp surface edges of TiO_2 become blurry for Pt–10Na, indicating multilayer deposition of Na species on the support and/or the segregation of Na species.

The difference of the Pt dispersions estimated from TEM and from CO chemisorption (Table 2) suggests the partial surface coverage of the Pt by NaO_x and/or TiO_x when the catalysts are reduced at 300 °C. For Pt–3Na, such coverage is estimated to be 23% (difference between D_{TEM} and D_{CO}), which can therefore provide a higher number of exposed Pt–NaO_x interface sites, where the WGS reaction may preferentially take place. The coverage is more pronounced for low and high Na loadings (Pt–1Na and Pt–10Na), which is harmful for WGS due to fewer exposed Pt surface atoms.

HR-TEM measurements were performed to examine the fine structure of Na-promoted Pt/TiO_2 catalysts. Pt–0Na and Pt–1Na show clean surface Pt particles (not shown). Compared to CO chemisorption, it may suggest a monolayer of Na coverage of Pt particles in Pt–1Na, which is difficult to be observed in TEM. Fig. 4 shows HR-TEM images for Pt–3Na and Pt–10Na. Well-resolved lattice fringes corresponding to anatase TiO_2 (1 0 1) and Pt (1 1 1) are clearly observed in both samples. The thin layers of NaO_x (lattice fringes are not resolved) are deposited over both TiO_2 and Pt for Pt–3Na (Fig. 4A). Multilayers of NaO_x coverage of both TiO_2 and Pt are easily observed for Pt–10Na. An example of fully covered Pt by NaO_x is shown in Fig. 4B, and partially covered Pt by NaO_x is shown in Fig. S2. The Na species appears to be poorly resolved lattice fringes, implying a feature of mixed species. Close examination reveals the presence of Na_2O_2, Na_2CO_3, NaOH (Fig. 4B

Table 2
Na/Pt molar ratio, specific surface area (S_{BET}), total pore volume (V_p), dispersion (D), turnover frequency (TOF), and apparent activation energy (E_a) of Na-promoted Pt/TiO_2 catalysts for WGS.

Sample	Na loading (mmol/g)	Na/Pt	S_{BET} (m^2/g)	V_p (cm^3/g)	Dispersion (%)		TOF [c] (s^{-1})		E_a [d] (kJ/mol)
					D_{CO} [a]	D_{TEM} [b]	250 °C	300 °C	
Pt–0Na	0	0	48	0.271	38.5	69	0.155	0.355	74
Pt–1Na	0.43	8	47	0.267	17.4	69	0.199	0.927	–
Pt–2Na	0.87	17	42	0.257	30.6	–	0.499	2.848	–
Pt–3Na	1.30	25	38	0.228	31.8	55	0.951	3.233	76
Pt–4Na	1.74	34	38	0.223	30.2	–	1.390	3.821	80
Pt–6Na	2.61	51	33	0.213	21.2	–	1.275	3.997	–
Pt–10Na	4.35	85	22	0.128	7.6	46	0.713	5.924	–

[a] Measured by CO chemisorption at room temperature.
[b] Estimated from $D = 100 \times 1.1/d_{TEM}$, where d_{TEM} is reported in Fig. 3.
[c] Measured under differential reaction conditions with CO conversion lower than 10%.
[d] Derived from Arrhenius plots measured under differential reaction conditions with CO conversion lower than 10% in the range of 200–300 °C.

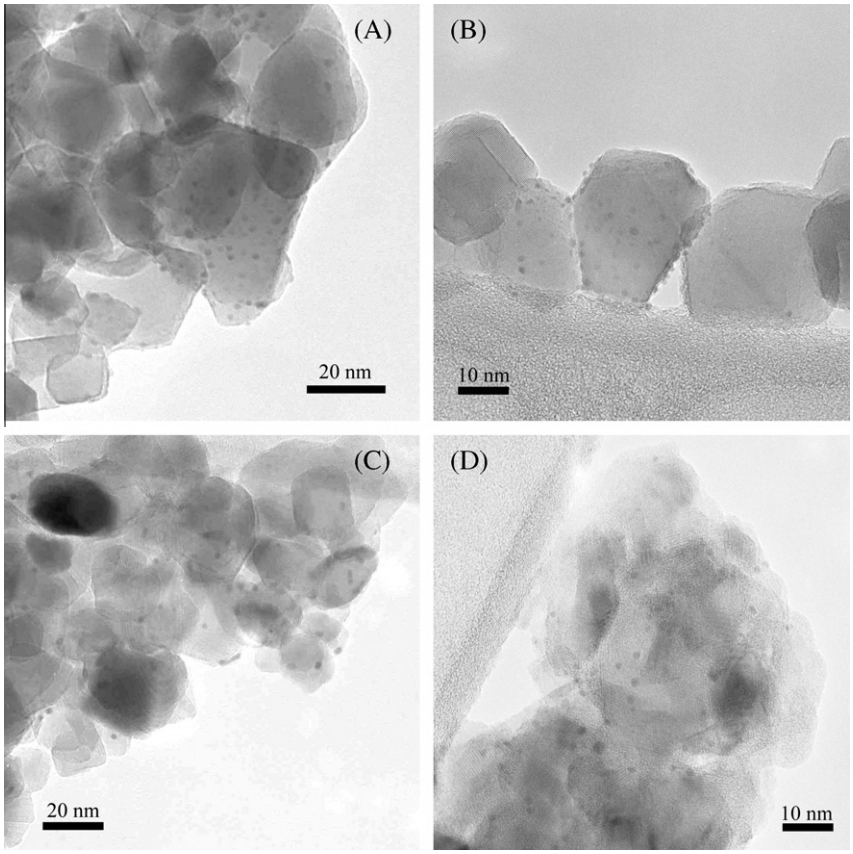

Fig. 2. TEM images of (A) Pt–0Na; (B) Pt–1Na; (C) Pt–3Na; and (D) Pt–10Na. Samples were reduced at 300 °C.

and Fig. S2). NaCl is also observed (Fig. S2); however, it is located away from the Pt particle. It should be noted that NaO_x species tend to be damaged with prolonged exposure to X-ray.

3.1.3. Reducibility

H_2-TPR is a useful tool to study metal–support interactions. Fig. 5 shows the H_2-TPR profiles of $Pt–Na/TiO_2$ catalysts as a function of Na loading; Table 3 lists the numerical results. In comparison, the H_2-TPR profiles of Na/TiO_2 samples are reported in Fig. S3. The addition of Na to Pt/TiO_2 improves the low-temperature reducibility significantly, indicating that addition of Na changes the metal–support interactions dramatically. For all samples, the profile can be roughly divided into two regions, low temperature (LT) (<250 °C) and high temperature (HT) (>250 °C), which can be related to reductions of Pt plus Na species [23,26] and of TiO_2 species [32,33], respectively. Reduction of Na/TiO_2 requires temperatures higher than 480 °C (Fig. S3). The presence of Pt in Na/TiO_2 shifts the reduction of Na species to significantly lower temperatures. Pt can form several states (Pt^0, PtO, PtO_2) over the support, depending on the calcination temperature, support properties, and metal–support interactions [33]. Generally, stronger metal–support interactions stabilize the Pt in a higher oxidation state. It should be noted that under the present conditions, some of the easily reduced Pt species (weak interaction with the support) have been reduced during the period of the TCD signal stabilization that takes place at room temperature and so do not appear at all.

In the LT region, the Pt species reduction peaks are weak and broad for sample Pt–0Na (curve a) and Pt–1Na (curve b), centered at 88 °C, indicating that most of the Pt species are reduced during the TCD signal stabilization (which is evidenced by a catalyst color

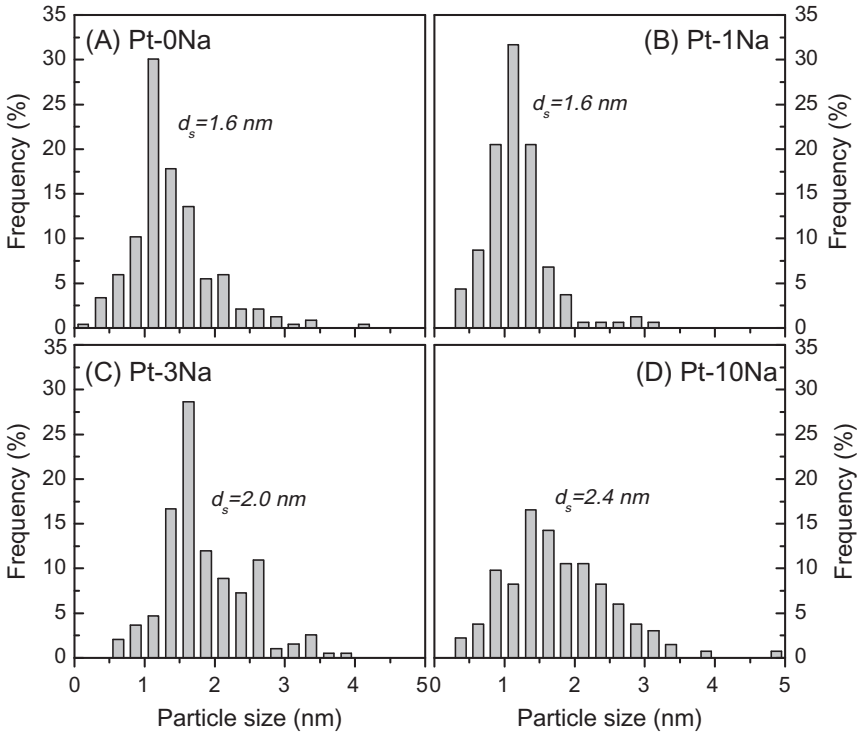

Fig. 3. Pt particle size distributions.

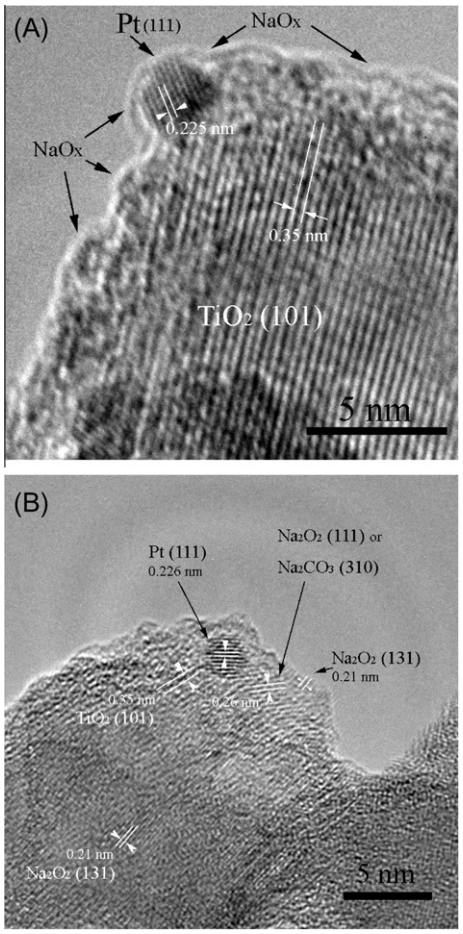

Fig. 4. HR-TEM images of (A) Pt–3Na and (B) Pt–10Na. Samples were reduced at 300 °C.

change from orange brown to dark grey for Pt–0Na and Pt–1Na during this process). Two sharp peaks at 88 and 137 °C are visible for Pt–2Na (curve c), which can be assigned to Pt species and Na species, respectively. The peak for Pt species shifts to higher temperature (98 °C) and overlaps with the peak of Na species for Pt–3Na (curve d), accompanied by increasing intensities for both species. The two peaks completely merge into one sharp, strong peak at 134 °C for Pt–4Na (curve e). The continued increase in peak intensity for the Pt species and the gradual shift of this peak to higher temperatures as Na loading increases indicate the development of strong metal–promoter interactions between Pt and Na species, which stabilizes the Pt species and in turn facilitates the reduction of Na species. Further increase in Na loading (Pt–6Na and Pt–10Na (curves f and g)) results in an increase in intensity of the reduction peak of Pt plus Na species, as well as the formation of a high-temperature shoulder (>200 °C, peak α in Fig. 5B). This shoulder may be assigned to the reduction of un-decomposed $NaNO_3$ or the Na species that are located away from the Pt particles.

In the HT region, one weak and broad peak (200–750 °C) is evidenced for the Pt–0Na (curve a), which possibly results from a combination of reductions of surface [30,31] and bulk TiO_2. The peak is separated into two well-defined regions of 300–550 °C (peak β in Fig. 5) and >600 °C (peak γ in Fig. 5) for Na-promoted samples, which are probably related to surface and bulk TiO_2 reductions, respectively. It is seen that the peak intensities increase and the peaks shift to higher temperatures as Na loading increases. This result suggests that Na addition inhibits the rate of hydrogen spillover from Pt to TiO_2 because of the interactions between Pt and Na species. However, it seems that addition of Na improves the degree of reduction of TiO_2 (Table 3). The peak at 500 °C for Pt–1Na may be associated with reduction of surface Na-modified TiO_2 species.

3.1.4. Surface basicity

As a product of WGS reaction, CO_2 can strongly affect catalyst performance through its adsorption properties [25,26,34]. The

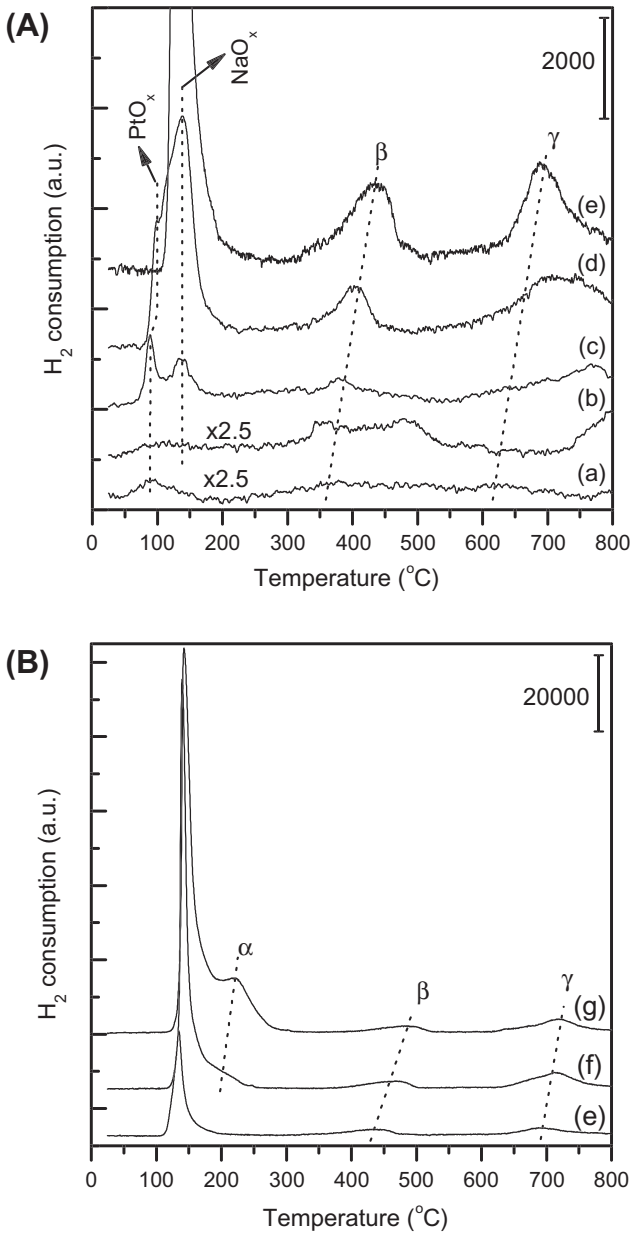

Fig. 5. H_2-TPR profiles of Na-promoted Pt/TiO_2 catalysts. Due to the significant variation of intensities for different samples, the figure is separated into (A) and (B), using Pt–4Na as a reference. (a) Pt–0Na; (b) Pt–1Na; (c) Pt–2Na; (d) Pt–3Na; (e) Pt–4Na; (f) Pt–6Na; (g) Pt–10Na.

surface basicity of $Pt–Na/TiO_2$ catalysts is investigated by CO_2-TPD, as shown in Fig. 6 and Table 4. In comparison, the CO_2-TPD profiles for TiO_2 and Na/TiO_2 are reported in Fig. S4, which suggests that the basicity is mainly from NaO_x species instead of Pt. Very weak adsorption of CO_2 on Pt–0Na (Fig. 6a) and Pt–1Na (Fig. 6b) is observed. This is in agreement with a kinetic study over Pt/TiO_2 showing 0 reaction order for CO_2 in the WGS reaction [35]. A strong peak <300 °C (peak α) is evidence that when Na loading is higher than 2 wt.%, the peak intensity is slightly increased with increased Na loading. However, two high-temperature peaks (peak β (350–500 °C) and peak γ (500–550 °C)) appear for Pt–2Na (Fig. 6c) and increase in intensity and shift to higher temperatures as Na loading increases (Fig. 6d–f). The peak α may be deconvoluted into weak- and medium-strength basic sites [25,26] and may be associated with the bicarbonate adsorbed on surface OH groups and bridged and bidentate carbonates adsorbed on $M^{x+}–O^{2-}$ pairs (M = Ti or Na in the present case), respectively [36–38]. The strongly binding sites (peak β and γ) may be unidentate carbonates strongly adsorbed on low-coordination O^{2-} ions [36,38,39] and/or formation of Na_2CO_3 [39]. The increase in O^{2-} ion concentration (related to oxygen vacancies) with increasing Na loading reflects high oxygen mobility of NaO_x species, thus easily participating in the WGS reaction by oxidation of CO to CO_2 [27]. In turn, high amounts of strongly binding carbonates may hinder the WGS reaction by slowing regeneration of these active sites.

3.1.5. Surface composition and Pt oxidation state

The surface composition and oxidation state of Pt before and after reduction were examined by XPS. Table 5 summarizes the

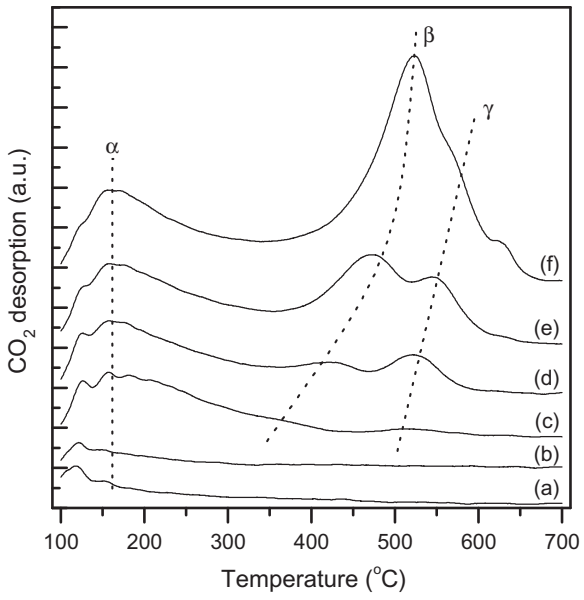

Fig. 6. CO_2-TPD profiles of (a) Pt–0Na; (b) Pt–1Na; (c) Pt–2Na; (d) Pt–3Na; (e) Pt–4Na; (f) Pt–6Na.

Table 3
Numerical results of H_2-TPR.

Sample	H_2 consumption (μmol/g)			
	<250 °C	Peak β	Peak γ	Total
Pt–0Na	18.7	98.9	–[a]	117.6
Pt–1Na	12.9	77.0	36.5[b]	126.5
Pt–2Na	145.3	30.9	210.2[b]	386.3
Pt–3Na	627.0	107.6	329.7[b]	1064.3
Pt–4Na	1387.9	292.9	334.2	2015.0
Pt–6Na	4294.7	297.6	741.7	5334.1
Pt–10Na	7784.1	322.9	687.0	8794.0

[a] Included in peak β.
[b] The peak is not complete at 800 °C.

Table 4
Numerical results of CO_2-TPD.

Sample	Desorbed CO_2 (μmol/g)			
	Peak α	Peak β	Peak γ	Total
Pt–0Na	9.1	0	0	9.1
Pt–1Na	22.7	0	0	22.7
Pt–2Na	141.4	12.8	8.6	162.8
Pt–3Na	144.2	30.7	33.3	208.3
Pt–4Na	173.3	138.4	72.8	384.5
Pt–6Na	185.7	356.4	85.5	625.6

surface composition. As Na loading is increased, the Pt concentration and Pt/Ti atomic ratio for samples both before and after reduction follow a similar trend as the Pt dispersion measured by CO chemisorption, but differs from that measured by TEM. The results imply that partial coverage of Pt species by NaO_x species has occurred, at least in part, during the catalyst preparation, leading to the formation of strong metal–promoter interactions between Pt and NaO_x species. This partial coverage not only provides active Pt–promoter interface sites for WGS reaction but also has been shown to stabilize Pt particles from sintering [29]. Such a strong metal–promoter interaction is different from the typical strong metal–support interaction (SMSI), which is formed only after reductions at elevated temperatures [40].

The surface concentrations of Cl and N are increased with increased Na loading. H_2 reduction reduced Cl to some extent and almost eliminated N. The residue Cl is most probably trapped by the surface of TiO_2 and NaO_x, instead of directly coordinated to Pt. If the latter was the case, it could be expected that the surface concentration of Cl should follow a similar trend as Pt due to the surface coverage. This is supported, in part, by HR-TEM results of the formation of NaCl on the catalyst surface, but away from Pt particle (Fig. S2). Furthermore, residual Cl does not appear to be inhibiting the WGS reaction. During the process of catalyst preparation, the ligand Cl^- coordinated with Pt^{4+} in the precursor is gradually replaced by OH^- and adsorbed on the support [41] and finally decomposed to O^{2-} during calcination. The released Cl may be retained by the support depending on the support properties [42,43]. This could be supported in part by the formation of NaCl observed in XRD (Fig. 1) and HR-TEM (Fig. S2).

Na addition changes the profiles of Pt 4f core electrons significantly. For the samples before reduction (Fig 7a), the BE of Pt 4f shifts to higher values with increasing Na loading. The shift in BE can be related to several factors, the oxidation state, the particle size of Pt, and the coordinated ligand to Pt (Cl or O) [44]. As discussed, Cl directly coordinating with Pt seems to have little influence on the Pt oxidation state. The effect of particle size can also be excluded since increasing Pt particle size with increasing Na loading is expected to result in electron enrichment of the particle and thus lower the BE. Therefore, the increase in BE of Pt is mainly associated with the oxidation state changes due to NaO_x addition. Curve fittings (Fig. 7a) clearly illustrate that the oxidation state changes from mainly Pt^{2+} (at 72.6 eV for Pt $4f_{7/2}$) for Pt/TiO_2 to mainly Pt^{4+} (at 74.5 eV for Pt $4f_{7/2}$) for Na-promoted samples (Table 5). This implies that the charge transfer from Pt to adjacent O of NaO_x species, i.e. formation of Pt–O–Na interactions, stabilizes Pt particles in higher oxidation states. The result indicates the formation of strong metal–promoter interactions between Pt and NaO_x species through Pt–O–Na, besides the physical coverage.

For the reduced samples (Fig 6b), besides the Pt^0 (at 71.1 eV for Pt $4f_{7/2}$), the content of cationic $Pt^{\delta+}$ (at 72.7 eV for Pt4/$f_{7/2}$) is present for all samples, increasing in intensity with increasing Na loading (Table 5). Though we cannot exclude the presence of $Pt^{\delta+}$ due to

Table 5
Surface composition derived from XPS.

Sample	State	Surface composition[a] (mol.%)						Atomic ratio			
		N	O	Na	Cl	Ti	Pt	Pt/Ti	Pt^{4+}/Pt^{2+}	$Pt^{\delta+}/Pt^0$	O_{II}/O_I
Pt–0Na	Oxidized	0.23	45.56	0	0.41	35.34	2.05	0.058	0.48		0.11
Pt–1Na	Oxidized	0.19	41.98	6.64	2.35	29.87	0.98	0.033	0.73		0.15
Pt–3Na	Oxidized	0.54	36.03	17.95	3.79	28.66	1.69	0.059	1.76		0.34
Pt–10Na	Oxidized	1.32	36.62	20.07	3.59	28.04	0.67	0.024	3.01		0.43
Pt–0Na	Reduced	0.01	48.06	0	0.24	35.06	1.40	0.040		0.75	0.13
Pt–1Na	Reduced	0.11	44.46	3.2	0.72	37.09	0.82	0.022		1.64	0.06
Pt–3Na	Reduced	0.05	38.05	15.43	2.71	29.06	1.16	0.040		1.92	0.26
Pt–10Na	Reduced	0.07	38.25	21.32	2.86	24.37	0.78	0.032		1.93	0.81

[a] Surface carbon is not reported.

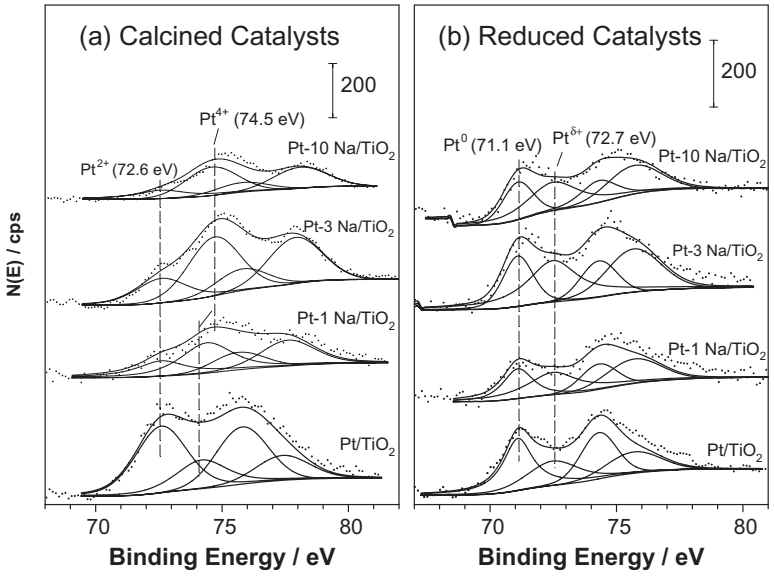

Fig. 7. XPS spectra of Pt 4f. Dots, experimental data; lines, curve fittings.

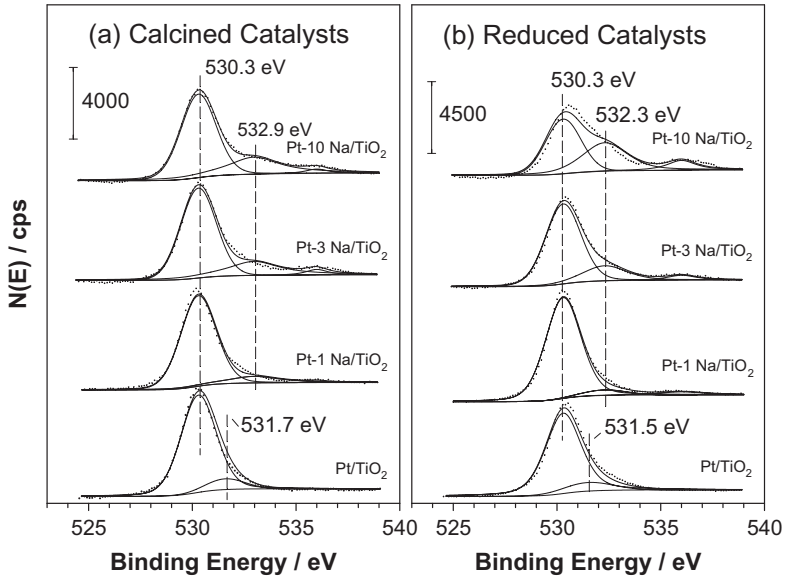

Fig. 8. XPS spectra of O 1s. Dots, experimental data; lines, curve fittings.

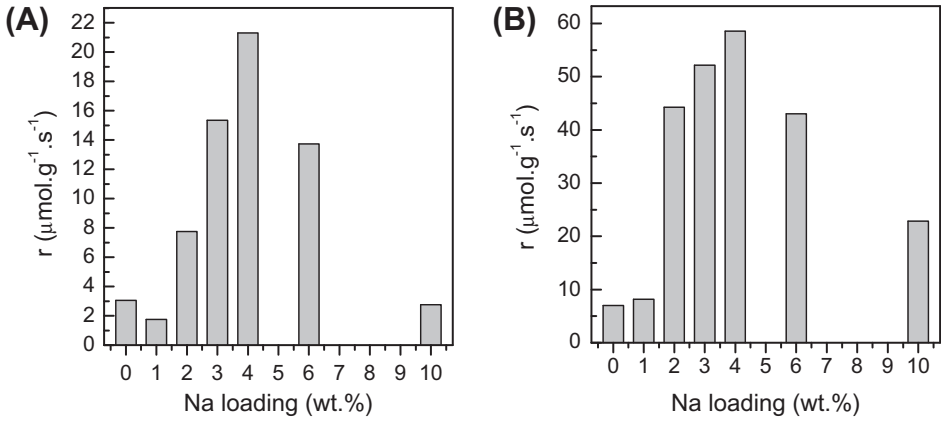

Fig. 9. Effect of Na loading on the intrinsic reaction rate of Na-promoted Pt/TiO_2 catalysts for WGS at (A) 250 °C and (B) 300 °C.

the oxidation of Pt by O_2 and H_2O in air during transfer of the sample to the XPS chamber, the increase in its intensity with Na loading reflects, at least in part, that high Na loading favors the formation of $Pt^{\delta+}$ due to the adjacent NaO_x. Again, these results imply the formation of strong metal–promoter interactions of Pt–O–Na, which helps the oxidation of the reduced support and Pt by water during reaction. The $Pt^{\delta+}$ is also believed to be an active species for the WGS reaction by some researchers [7].

The XPS of O 1s provides additional information (Fig. 8). The peak at BE of 530.3 eV can be assigned to lattice oxygen of bulk TiO_2 (O_I); the shoulder peak at BE of 531.5 eV could be assigned to surface oxygen species (O_{II}) for Pt/TiO_2 (surface –OH of TiO_2) [45]. The shoulder peak (O_{II}) of Na-promoted samples is present at BE of 532.9 and 532.2 eV for samples before and after reduction, respectively. The broad feature of this peak implies that it contains more than one O species associated with Na, such as surface O in NaO_x, –OH, and carbonates. A weak peak at BE of 536 eV is present only for Na-containing samples that may be ascribed to adsorbed O_2 [46]. In line with H_2-TPR results, the O_{II} increases with Na loading (Table 5), implying these active O species may participate in the catalytic cycle [21].

3.2. Catalytic activity

The effect of Na loading on the intrinsic reaction rate was measured under differential reaction conditions at 250 and 300 °C. The results are plotted in Fig. 9 with the corresponding TOF listed in Table 2. It is seen that the amount of Na loading strongly affects the catalytic performance. Low Na loading (Pt–1Na) has even a negative effect on the WGS activity. The Na/Pt ratio of 8 for Pt–1Na falls into the range that has been shown to have a negative effect for alkali-promoted catalysts for WGS [25,26,28] (and also for CO oxidation [30]). However, increasing Na loading (Pt–2Na, Pt–3Na, and Pt–4Na) improves the WGS activity significantly, with maximum improvement achieved for 3–4 wt.% Na loading. At 250 °C, the intrinsic reaction rate is improved by 5 and 7 times for Pt–3Na and Pt–4Na (Fig. 9A), respectively. Correspondingly, the TOF is improved by a factor of 6 and 9 times. At 300 °C, the intrinsic reaction rate is improved 7 and 8 times for Pt–3Na and Pt–4Na (Fig. 9B), respectively, with a TOF improvement of 9 and 11 times. Further increases in Na loading (Pt–6Na and Pt–10Na) reduce the improvement factor, possibly related to both reduction in surface Pt and excessively strong adsorption of surface carbonates.

The intrinsic reaction rate and TOF of high Na loading samples (Pt–6Na and Pt–10Na) increases relative to those of Pt–4Na, when the reaction temperature is increased from 250 to 300 °C. This improvement could result from higher temperatures that facilitate the decomposition of carbonates in the presence of water [47].

The Arrhenius plots of intrinsic reaction rate over Pt–0Na, Pt–3Na, and Pt–4Na catalysts in the reaction temperature range of 200–300 °C are displayed in Fig. 10. The intrinsic reaction rates are improved significantly with Na addition over the entire temperature range tested. The apparent activation energies (E_a) for the WGS reaction were obtained from the fitted slopes in Fig. 10 and are reported in Table 2. The E_a vary from 74–80 kJ/mole in agreement with the literature [28] and are found to be slightly higher for the Na-promoted samples.

3.3. Discussion

The titration of surface –OH by alkaline metals is well illustrated in the literature [48]. The surface –OH concentration is estimated to be 6 nm^{-2}, or 0.5 mmol/g for TiO_2 [27]. Loading 1 wt.% Na titrates ~85% of surface of –OH (formation –ONa), forming near monolayer coverage of the support, which has little influence on the physical adsorption and surface basicity properties. The monolayer Na also partially covers the Pt surface and leads to higher oxidation states of Pt. However, the interaction between Pt and Na appears relatively weak, as evidenced by the H_2-TPR, showing that most Pt species are reduced at room temperature. When Na loading exceeds the monolayer coverage, the physical adsorption and surface basicity properties change significantly. Moderate increase in Na loading (2–4%, forming 2–4 layers of NaO_x on TiO_2 support) forms the strong metal–promoter interactions between Pt and Na species through Pt–O–Na interactions. Further increase in Na loading (>4%, resulting in multilayer NaO_x on TiO_2) leads to low surface area, low fraction of exposed Pt, and high surface basicity.

Additional experiments of CO chemisorption measuring Pt dispersions for the Pt–0.5Na and Pt–1.5Na samples gave values of 26.7% and 25.1%, respectively, suggesting there seems to be a minimum Pt dispersion around 1 wt.% Na loading. Since TEM measurement showed similar Pt particle sizes for Pt–0Na and Pt–1Na, this minimum dispersion should result from monolayer Na species coverage of Pt. Note that the dispersion measured by CO chemisorption is quite reproducible; this minimum seems to be related to the properties of the precursors and support and the chemistry during impregnation, but has not been a subject of this study.

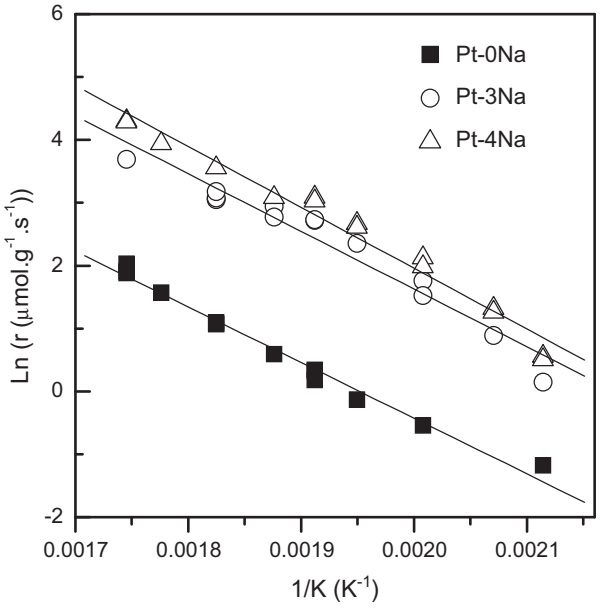

Fig. 10. Arrhenius plots of intrinsic reaction rates over Pt–0Na, Pt–3Na, and Pt–4Na catalysts in the reaction temperature range of 200–300 °C.

The major reaction pathways proposed for the WGS reaction over Pt supported on reducible oxides are an associative pathway with interaction of CO on Pt with –OH on the support leading to formation of surface formate, which then decomposes to CO_2 and H_2 [49]; a redox pathway, where CO on Pt is oxidized by O from the support to form CO_2 and the resulting oxygen vacancy, is refilled by H_2O, releasing H_2 [6]. The dominant reaction pathway is strongly dependent on the reaction conditions, i.e. low temperature and high H_2O/CO ratio favor the associative path while high temperature and low H_2/CO favor the redox path [3]. However, in both reaction pathways, CO is adsorbed on Pt while H_2O is activated on the support, and the reaction takes place on Pt–support sites at the periphery of the interface. Thus, the Pt dispersion, properties of the support, and the number of exposed Pt–support interfacial sites are important for WGS activity.

The literature has shown that addition of alkali promotes the activation of water [21], the formation of formate [50], the decomposition of the C–H bond of formate [23–26], and formation of oxygen vacancies at the Pt–support interface [27,28]. It is evident that maximizing the promotional role of Na is strongly dependent on the configuration of Pt–promoter interactions. The strong metal–promoter interactions between Pt and Na species have been demonstrated by the data from TEM, CO chemisorption, TPR, and XPS, when 2–4 wt.% Na has been added. The TPR results have shown that these strong metal–promoter interactions improve the low-temperature reducibility significantly, thus facilitating the formation of oxygen vacancies and further improving the H_2O dissociation on these vacancies. The optimal coverage of the Pt surface by Na species provides a greater exposed Pt–NaO_x interface for the WGS reaction, resulting in significant improvement in WGS activity. However, these improvements are balanced by both the exposed Pt surface and the formation of relatively inert carbonates due to higher alkalinity [21,23–26], and thus, too high of a Na loading was found to reduce the activity improvement.

Compared to promoted Pt/TiO_2 and Pt/CeO_2 catalysts reported recently in the literature (Table 1), the promotional effects of Na for Pt–4Na on the intrinsic reaction rate and TOF are significantly higher in this study. It should be noted that comparison of the absolute values of reaction rate and TOF is not straight forward, since they are strongly influenced by reaction conditions (composition, pressure, temperature). The promotional effect is also significantly higher than Na-promoted Pt/TiO_2 prepared by sequential impregnations [28]. Note that the absolute reaction rate is higher in [28] due to higher H_2O/CO ratio and absence of H_2 used in the feed (Table 1). This difference could be expected if, as a result of sequential impregnation, this only modifies the interface between Pt and the TiO_2 support. Co-impregnation apparently leads to better metal–promoter interactions at not only the Pt–TiO_2 interface but also because of partial coverage of the Pt surface by NaO_x.

An interesting comparison may be made between Pt–1Na and Pt–10Na. Pt–10Na has a lower fraction of exposed Pt but has higher intrinsic reaction rate and TOF than Pt–1Na. It is expected that monolayer coverage of the support titrates the surface Ti–OH to Ti–O–Na [48], and this reduces the active oxygen species from the TiO_2 support that participate in the bifunctional reaction cycle. While at the same time, the active oxygen species in NaO_x adjacent to Pt cannot compensate for the loss of Ti–OH at this condition. Thus, the activity is somewhat lower. These results are in good agreement with literature results showing the negative effect when the Na/Pt ratio is higher than 1 [25,26,28]. However, with further increase in Na loading, the adjacent NaO_x provide sufficient active oxygen species for the bifunctional reaction, resulting in

significant improvement in activity. Therefore, Pt–10Na appears to be more active than Pt–1Na.

The maximum improvement is achieved over Pt–4Na under the conditions of the present study, which is somewhat different from previous work that showed a maximum improvement over Pt–3Na [29]. The CO concentration (30%) and conversion level (near equilibrium) in the previous study [29] were significantly higher than in this study. As a consequence, the CO_2 concentration was much higher than present conditions. It could be expected that the improvement was balanced by the inhibition of the high concentration of CO_2 due to greater adsorption of CO_2 over Pt–4Na than over Pt–3Na. These differences suggest that the catalyst can be optimized for the specifications of the reaction system, e.g., water/CO ratio, CO_2 partial pressure, temperature, residual CO level, etc.

4. Conclusions

Intrinsic reaction rate measurements of the water gas shift reaction under differential reaction conditions showed that addition of 3–4 wt.% Na promotes the 1% Pt/TiO_2 activity significantly. The intrinsic reaction rate is improved by a factor of 8 for 1%Pt–4%Na/TiO_2 at 300 °C, with a corresponding improvement in turnover frequency by a factor of 11. With 2–4 wt.% Na addition, 2–4 layers of NaO_x were deposited on the support, and the Pt particles were partially covered by NaO_x, with moderate surface basicity and exposed Pt surface areas. The interactions between Pt and NaO_x may occur by Pt electron donation to O in NaO_x through Pt–O–Na. The strong metal–promoter interactions between Pt and Na species stabilize Pt in higher oxidation states and facilitate the reduction of Na species. The low-temperature reducibility is thus improved significantly, which is beneficial for the reaction by either an associative reaction path or a redox path. Higher amounts of exposed Pt–NaO_x sites at the interface with the support enhance the WGS reaction and also have been shown to inhibit Pt particles from sintering. The significant improvement in WGS activity of Pt–Na/TiO_2 catalysts, accompanied by operation under severe conditions with a space velocity up to 40,000 $cm^3 \cdot g_{cat}^{-1} \cdot h^{-1}$ [29], may provide potential candidates for highly active and stable WGS catalyst for small-scale applications that can be tuned to the needed reaction conditions.

Acknowledgments

Support from SEMGREEN, LP is greatly appreciated. Several characterizations were performed in Prof. D.E. Resasco's Lab, which are greatly appreciated. The authors thank Gregory W. Strout for his help with TEM measurements.

Appendix A. Supplementary material

Supplementary data associated with this article can be found, in the online version, at doi:10.1016/j.jcat.2010.11.023.

References

[1] C. Ratnasamy, J.P. Wagner, Catal. Rev. 51 (2009) 325. and references therein.
[2] G. Jacobs, B.H. Davis, Catalysis 20 (2007) 122. and references therein.
[3] R. Burch, Phys. Chem. Chem. Phys. 8 (2006) 5483. and references therein.
[4] O. Thinon, F. Diehl, P. Avenier, Y. Schuurman, Catal. Today 137 (2008) 29.
[5] P. Panagiotopoulou, D.I. Kondarides, Catal. Today 112 (2006) 49.
[6] T. Bunluesin, R.J. Gorte, G.W. Graham, Appl. Catal. B 15 (1998) 107.
[7] Y.P. Zhai, D. Pierre, R. Si, W.L. Deng, P. Ferrin, A.U. Nilekar, G.W. Peng, J.A. Herron, D.C. Bell, H. Saltsburg, M. Mavrikakis, M. Flytzani-Stephanopoulos, Science 329 (2010) 1633.
[8] H. Iida, A. Igarashi, Appl. Catal. A 298 (2006) 152.
[9] K.G. Azzam, I.V. Babich, K. Seshan, L. Lefferts, J. Catal. 251 (2007) 163.
[10] Y. Sato, K. Terada, S. Hasegawa, T. Miyao, S. Naito, Appl. Catal. A 296 (2005) 80.
[11] R. Radhakrishnan, R.R. Willigan, Z. Dardas, T.H. Vanderspurt, Appl. Catal. B 66 (2006) 23.
[12] S.Y. Choung, M. Ferrandon, T. Krause, Catal. Today 99 (2005) 257.
[13] X.L. Zhu, T. Hoang, L.L. Lobban, R.G. Mallinson, Appl. Catal. B 94 (2010) 311.
[14] A.M.D. de Farias, A.P.M.G. Barandas, R.F. Perez, M.A. Fraga, J. Power Sour. 165 (2007) 854.
[15] A.M.D. de Farias, P. Bargiela, M.daGraçaC. Rocha, M.A. Fraga, J. Catal. 260 (2008) 93.
[16] I.D. González, R.M. Navarro, W. Wen, N. Marinkovic, J.A. Rodriguéz, F. Rosa, J.L.G. Fierro, Catal. Today 149 (2010) 372.
[17] Y.T. Kim, E.D. Park, H.C. Lee, D. Lee, K.H. Lee, Appl. Catal. B 90 (2009) 45.
[18] J.B. Park, J. Graciani, J. Evans, D. Stacchiola, S.D. Senanayake, L. Barrio, P. Liu, J.F. Sanz, J. Hrbek, J.A. Rodriguez, J. Am. Chem. Soc. 132 (2010) 356.
[19] W. Ruettinger, X.S. Liu, X.M. Xu, R.J. Farrauto, Top. Catal. 51 (2008) 60.
[20] A. Gayen, M. Boaro, C. de Leitenburg, J. Llorca, A. Trovarelli, J. Catal. 270 (2010) 285.
[21] J.M. Campbell, J. Nakamura, C.T. Campbell, J. Catal. 136 (1992) 24.
[22] S. Sato, J.M. White, J. Catal. 69 (1981) 128.
[23] J.M. Pigos, C.J. Brooks, G. Jacobs, B.H. Davis, Appl. Catal. A 319 (2007) 47.
[24] J.M. Pigos, C.J. Brooks, G. Jacobs, B.H. Davis, Appl. Catal. A 328 (2007) 14.
[25] H.N. Evin, G. Jacobs, J. Ruiz-Martinez, G.A. Thomas, B.H. Davis, Catal. Lett. 120 (2008) 166.
[26] H.N. Evin, G. Jacobs, J. Ruiz-Martinez, U.M. Graham, A. Dozier, G. Thomas, B.H. Davis, Catal. Lett. 122 (2008) 9.
[27] P. Panagiotopoulou, D.I. Kondarides, J. Catal. 260 (2008) 141.
[28] P. Panagiotopoulou, D.I. Kondarides, J. Catal. 267 (2009) 57.
[29] X.L. Zhu, T. Hoang, L.L. Lobban, R.G. Mallinson, Catal. Lett. 129 (2009) 135.
[30] H. Tanaka, M. Kuriyama, Y. Ishida, S.-i. Ito, T. Kubota, T. Miyao, S. Naito, K. Tomishige, K. Kunimori, Appl. Catal. A 343 (2008) 125.
[31] R. Pellegrini, G. Leofanti, G. Agostini, L. Bertinetti, S. Bertarione, E. Groppo, A. Zecchina, C. Lamberti, J. Catal. 267 (2009) 40.
[32] T. Huizinga, J. Van Grondelle, R. Prins, Appl. Catal. 10 (1984) 199.
[33] P. Panagiotopoulou, A. Christodoulakis, D.I. Kondarides, S. Boghosian, J. Catal. 240 (2006) 114.
[34] A.A. Phatak, N. Koryabkina, S. Rai, J.L. Ratts, W. Ruettinger, R.J. Farrauto, G.E. Blau, W.N. Delgass, F.H. Ribeiro, Catal. Today 123 (2007) 224.
[35] C.M. Kalamaras, P. Panagiotopoulou, D.I. Kondarides, A.M. Efstathiou, J. Catal. 264 (2009) 117.
[36] J.I. Di Cosimo, V.K. Díez, M. Xu, E. Iglesia, C.R. Apesteguía, J. Catal. 178 (1998) 499.
[37] F. Prinetto, M. Manzoli, S. Morandi, F. Frola, G. Ghiotti, L. Castoldi, L. Lietti, P. Forzatti, J. Phys. Chem. C 114 (2010) 1127.
[38] E.L. Kunkes, E.I. Gürbüz, J.A. Dumesic, J. Catal. 266 (2009) 236.
[39] Z.L. Zhang, Y.X. Zhang, Z.P. Wang, X.Y. Gao, J. Catal. 271 (2010) 12.
[40] G.L. Haller, D.E. Resasco, Adv. Catal. 36 (1989) 173.
[41] B. Shelimov, J.-F. Lambert, M. Che, B. Didillon, J. Catal. 185 (1999) 462.
[42] H. Karhu, A. Kalantar, I.J. Väyrynen, T. Salmi, D.Yu. Murzin, Appl. Catal. A 247 (2003) 283.
[43] A. Holmgren, B. Andersson, D. Duprez, Appl. Catal. B 22 (1999) 215.
[44] J. Silvestre-Albero, A. Sepúlveda-Escribano, F. Rodríguez-Reinoso, J.A. Anderson, J. Catal. 223 (2004) 179.
[45] J. Ruiz-Martinez, A. Sepúlveda-Escribano, J.A. Anderson, F. Rodríguez-Reinoso, Phys. Chem. Chem. Phys. 11 (2009) 917.
[46] A.J. Plomp, D.S. Su, K.P. de Jong, J.H. Bitter, J. Phys. Chem. C 113 (2009) 9865.
[47] G. Jacobs, P.M. Patterson, L. Williams, D. Sparks, B.H. Davis, Catal. Lett. 96 (2004) 97.
[48] A. Iordan, M.I. Zaki, C. Kappenstein, J. Chem. Soc. Faraday Trans. 89 (1993) 2527.
[49] G. Jacobs, U.M. Graham, E. Chenu, P.M. Patterson, A. Dozier, B.H. Davis, J. Catal. 229 (2005) 499.
[50] Y. Amenomiya, G. Pleizier, J. Catal. 76 (1982) 345.